AAC Accepted Manuscript Posted Online 8 January 2018
Antimicrob. Agents Chemother. doi:10.1128/AAC.02063-17

Novel Pyrimidines as Antitubercular Agents

Daigo Inoyama[1,*], Steven D. Paget[1,*,&], Riccardo Russo[2], Srinivasan Kandasamy[1], Pradeep Kumar[2], Eric Singleton[2], James Occi,[2] Margareta Tuckman[2], Matthew D. Zimmerman[3], Hsin Pin Ho[3], Alexander L. Perryman[1], Véronique Dartois[3], Nancy Connell[2], and Joel S. Freundlich[1,2,#]

1. Department of Pharmacology, Physiology and Neuroscience, Rutgers University – New Jersey Medical School, Newark, New Jersey, USA.

2. Division of Infectious Disease, Department of Medicine and the Ruy V. Lourenço Center for the Study of Emerging and Re-emerging Pathogens, Rutgers University - New Jersey Medical School, Newark, New Jersey USA.

3. Public Health Research Institute, Rutgers University – New Jersey Medical School, Newark, New Jersey, USA.

[#] Address correspondence to Joel S. Freundlich, freundjs@rutgers.edu.

Running Head: Antitubercular pyrimidines

Keywords: *Mycobacterium tuberculosis*, antitubercular, pyrimidine, pharmacokinetics.

[*] D.I. and S.D.P. contributed equally to this work.

[&] Present address: Venenum BioDesign, Hamilton, NJ, USA.

ABSTRACT

Mycobacterium tuberculosis infection is responsible for a global pandemic. New drugs are needed that lack cross-resistance with the existing front-line therapeutics. A triazine antitubercular hit led to the design of a related pyrimidine family. The synthesis of a focused series of these analogs facilitated exploration of their *in vitro* activity, *in vitro* cytotoxicity, physiochemical, and Absorption-Distribution-Metabolism-Excretion properties. Select pyrimidines were then evaluated for their mouse pharmacokinetic profiles. The findings suggest a rationale for the further evolution of this promising series of antitubercular small molecules, which appear to share some similarities with the clinical compound PA-824 in terms of activation, while highlighting more general guidelines for the optimization of small molecule antituberculars.

INTRODUCTION

Infection with *Mycobacterium tuberculosis* is responsible for tuberculosis (TB), a disease of global significance which infects nearly nine million people and kills 1.4 million people on an annual basis.(1) Despite whole-cell high-throughput phenotypic screening of nearly a million compounds from both commercial and pharmaceutical libraries, the TB drug discovery pipeline still suffers from a dearth of validated therapeutic strategies comprised of novel biological targets and high-quality small molecules that modulate them.(2) Our laboratory has been focused on leveraging novel computational techniques to discover, and in some cases re-discover, antitubercular chemotypes as growth inhibitors of *M. tuberculosis*.(3) We assert that growth inhibitors with new chemical scaffolds should have a heightened probability of interfering with the native function of *M. tuberculosis* proteins outside the sphere of inhibition of our current set of antitubercular drugs and chemical tools.

Our use of naïve Bayesian models (heretofore referred to as Bayesian models) trained with screening data for *M. tuberculosis* growth inhibition and Vero cell cytotoxicity from the Southern Research Institute led to the re-discovery of diaminotriazine nitrofurylhydrazones as potent growth inhibitors of *in vitro* cultured *M. tuberculosis*. Our initial profiling of TCMDC-125802 (renamed, JSF-2019; Fig. 1) found the molecule to exhibit a favorable lack of cytotoxicity to Vero cells and mouse bone marrow macrophages in addition to tolerability in mice, but failed to demonstrate *in vivo* efficacy in a γ interferon gene disrupted C57BL/6 mouse model of *M. tuberculosis* infection.(4) Efforts in our laboratories to explore the structure-activity relationships (SAR) pertinent to this series led to pyrimidine analogs. An exploratory set of pyrimidines is described herein, detailing their SAR pertinent to *in vitro* activity, Vero cell

cytotoxicity, physiochemical properties, *in vitro* Absorption-Distribution-Metabolism-Excretion (ADME), and mouse pharmacokinetics (PK).

MATERIALS AND METHODS

Chemistry: The synthesis of all pyrimidine molecules in this study was adapted from published methods and is detailed in the Supplementary Materials.

Determination of minimum inhibitory concentration (MIC) against *M. tuberculosis*: The *M. tuberculosis* H37Rv strain was grown in 7H9 broth (Becton, Dickinson and Company 271310), plus 0.2% glycerol (Sigma G5516), 0.25% Tween 80-20% (Sigma P8074) and 20% 5x ADC. The 5x ADC solution was prepared using 25 g/L Bovine Serum Albumin (Sigma A9647), 10g/L dextrose (Sigma D9434), and 4.2 g/L NaCl (Sigma S5886). Each compound was dissolved in DMSO at a final concentration of 12 mg/mL and serial dilutions were performed to generate typical test concentrations ranging from 50 – 0.024 μg/mL. As appropriate, further dilutions were made to determine an accurate MIC. *M. tuberculosis* strain H37Rv at the mid-logarithmic stage of growth (OD_{580} = 0.4) was diluted 1:100 and 0.1 mL was added to each well of a 96-well plate along with 0.1 mL of test compound solution. After 6 days of incubation at 37 °C, Alamar Blue (Invitrogen, Grand Island, NY) reagent was added along with 12.5 μL of 20% Tween 80 (Sigma, St. Louis, MO) to evaluate bacterial cell viability. Plates were scanned 24 h later at 570 nm with a reference wavelength of 600 nm utilizing a Biotek Instruments ELX 808. Inoculum control wells of untreated H37Rv were used to create a survival inhibition curve with each assay. Rifampicin was used as a positive control (MIC = 0.0125 - 0.05 μg/mL).

Determination of minimum bactericidal concentration (MBC) against *M. tuberculosis*: To determine the minimum bactericidal concentration (MBC) against *M. tuberculosis*, the bacterial cultures from the 96-well plates used for the compound MIC determination instead of undergoing Alamar Blue addition were re-suspended, serially diluted with sterile PBS and plated on Middlebrook 7H11 plates. Colony Forming Units (CFUs) were enumerated following 21-day incubation at 37 °C. The MBC was reported as the minimum compound concentration at which a 2 $\log_{10}$ reduction in CFUs was observed as compared to the no-compound control.

Determination of kinetics of cidality against *M. tuberculosis*: Determination of kinetics of cidality against *M. tuberculosis*: A 10 mL culture of *M. tuberculosis* H37Rv was grown up to an OD_{600} of 0.6-0.8 in Middlebrook 7H9 medium supplemented with 10% ADS (albumin, dextrose, sodium chloride), 0.25% glycerol and 0.05% Tween-80. The cells were harvested by centrifugation, washed twice with Middlebrook 7H9 plus ADS without any detergent and the pellet was resuspended in 10 mL of the same media. The cells were then diluted (1:100) and 100 µL aliquots of cells were added to wells in a 96-well plate. Stock solutions of isoniazid, JSF-2371, JSF-2245 and JSF-2019 were prepared in DMSO, and concentrations of 10X, 30X and 60X of the respective MIC for each compound were prepared in 7H9 plus ADS media. 100 µL of drug solution was added to the appropriate wells. The plates were incubated at 37 °C, aliquots were removed from each culture at different time points, serially diluted and plated on Middlebrook 7H10 agar plates to determine the CFUs.

Physiochemical and ADME profiling: This set of studies was performed by BioDuro, Incorporated. Published protocols were utilized to determine mouse and human liver microsomal

stability,(5) kinetic solubility,(6) Caco-2 permeability,(7) mouse plasma protein binding,(8) and human cytochrome P450 inhibition.(9)

Determination of efficacy in an intracellular infection model: The activity of JSF-2371 against intracellular bacteria was determined by infecting J774.1 mouse macrophages (ATCC TIB-67) with the mc^{2}6206 Δ*leuCD* Δ*panCD* strain of *M. tuberculosis* transformed with an mLux plasmid (kindly provided by Professor Jeffery Cox, UC Berkeley) based on published protocols.(10, 11) The infected macrophages were exposed to JSF-2371, rifampicin, or no drug for 72 h. Luminescence was measured every 24 h and viable bacteria inside the macrophages were recovered at the end of the experiment. The macrophages were suspended in Dulbecco's Modified Eagle Medium (Sigma-Aldrich D6429) supplemented with 10% Fetal Bovine Serum (Sigma-Aldrich F6178) to a concentration of 1.0 – 2.0 x 10^5 cells/mL. 96-well white flat-bottomed assay plates were seeded with 100 μL of the macrophage suspension and incubated overnight to allow cells to adhere to the plate. The assay plates were then inoculated with 100 μL of luminescent mc^{2}6206 *M. tuberculosis* at a multiplicity of infection of 1:1. The plates were incubated for 4 h at 37 °C and 5% CO_2 to allow the bacteria to infect the macrophages and then washed twice with 100 μL of DMEM supplemented with FBS, pantothenic acid and leucine. After the second wash, 100 μL of DMEM with gentamicin was added to each well and the plates were incubated for an additional 2 h to kill any remaining extracellular bacteria. The plates were washed twice with 100 μL of DMEM supplemented with FBS, pantothenic acid and leucine, and then JSF-2371 or rifampicin was added to the plates at the desired concentrations. The plates were incubated at 37 °C and 5% CO_2 for 72 h. Luminescence was measured every 24 h using the GloMax® Detection System (Promega). Each treatment was done in triplicate and the

experiment was repeated twice. To determine the number of live bacteria present in macrophages after 72 h from infection, macrophages were washed with warm PBS and then lysed by adding 200 μL of 0.02% Triton X-100 (Sigma-Aldrich X100) to the wells. The plates were incubated for 15 min at room temperature and then wells were mixed vigorously by pipetting to release intracellular bacteria. Serial dilutions of the lysed macrophages were prepared and plated on 7H10 agar plates. The plates were incubated at 37 °C for 3 weeks and then counted for colonies.

Mouse pharmacokinetics (PK) studies

Animals and ethics assurance: Animal studies were carried out in accordance with the guide for the care and use of Laboratory Animals of the National Institutes of Health, with approval from the Institutional Animal Care and Use Committee (IACUC) of the New Jersey Medical School, Rutgers University, Newark. All animals were maintained under specific pathogen-free conditions and fed water and chow *ad libitum*, and all efforts were made to minimize suffering or discomfort. In the 5 h PK studies, two female CD-1 mice received a single dose of experimental compound administered orally at 25 mg/kg in 5% DMA/60% PEG300/35% D5W (5% dextrose in water), and blood samples were collected in K_2EDTA coated tubes pre-dose, 0.5, 1, 3 and 5 h post-dose. In iv/po PK studies, groups of three female CD-1 mice received a single dose of experimental compound administered orally at 25 mg/kg in 0.5% CMC/0.5% Tween 80 suspension, or intravenously at 5 mg/kg in 5% DMA/95% (4 % Cremophor EL). Blood samples were collected in K_2EDTA coated tubes 0.25, 0.5, 1, 3, 5 and 8 h post-dose in the oral arm, and 0.033, 0.25, 0.5, 1 and 3 h post dose in the intravenous arm. Blood was kept on ice and centrifuged to recover plasma, which was stored at -80 °C until analyzed by HPLC coupled to tandem mass spectrometry (LC-MS/MS).

LC/MS-MS analytical methods: LC/MS-MS quantitative analysis for all molecules was performed on a Sciex Applied Biosystems Qtrap 4000 triple-quadrupole mass spectrometer coupled to an Agilent 1260 HPLC system, and chromatography was performed on an Agilent Zorbax SB-C8 column (2.1x30 mm; particle size, 3.5 µm) using a reverse phase gradient elution. Milli-Q deionized water with 0.1% formic acid (A) was used for the aqueous mobile phase and 0.1% formic acid in acetonitrile (B) for the organic mobile phase. The gradient was: 5-90% B over 2 min, 1 min at 90% B, followed by an immediate drop to 5% B and 1 min at 5% B. Multiple-reaction monitoring of parent/daughter transitions in electrospray positive-ionization mode was used to quantify all molecules. Sample analysis was accepted if the concentrations of the quality control samples and standards were within 20% of the nominal concentration (Quality control statistics may be found in Supplementary Table 3). Data processing was performed using Analyst software (version 1.6.2; Applied Biosystems Sciex). Neat 1 mg/mL DMSO stocks for all compounds were first serial diluted in 50/50 acetonitrile/water and subsequently serial diluted in drug free CD-1 mouse plasma (K_2EDTA, Bioreclamation IVT, NY) to create standard curves (linear regression with 1/x^2 weighting) and quality control (QC) spiking solutions. 20 µL of standards, QCs, control plasma, and study samples were extracted by adding 200 µL of acetonitrile/methanol 50/50 protein precipitation solvent containing the internal standard (10 ng/mL verapamil). Extracts were vortexed for 5 minutes and centrifuged at 4000 rpm for 5 minutes. 100 µL of supernatant was transferred for HPLC-MS/MS analysis and diluted with 100 µL of Milli-Q deionized water.

RESULTS

171 Initial design considerations for interrogation of the SAR around JSF-2019 led to
172 consideration of pyrimidine analogs. The pyrimidine analogs initially featured the same
173 substituents as the original hit (JSF-2019) at the R^1, R^2, and R^3 positions to determine the effect
174 of replacing the triazine core with pyrimidine. The pyrimidine core can possess the 5-nitrofuryl
175 hydrazone at either the 2- or 6-position with respect to the heteroatoms of the pyrimidine ring
176 (Figure 1), giving rise to two regioisomers. The dual-event Bayesian model (TAACF-CB2) that
177 predicted JSF-2019 as an active made similar projections for both pyrimidines (Supplementary
178 Table 1) based on their Bayesian scores (1.93 and 1.55 for the 2- and 6-hydrazone substituted
179 pyrimidines, respectively) exceeding the established cutoff for an active (0.427).(3) Importantly,
180 all three compounds exhibited calculated closest distance values of 0.887 – 0.893, indicative that
181 they are structurally quite dissimilar from the Bayesian model's training set.

182 The two regioisomeric pyrimidine analogs of JSF-2019 were synthesized following the
183 reaction schemes as outlined in Figures 2 and 3. Crucial to the approach was reliance on a
184 published strategy for control of the regioselectivity of amine additions to commercially
185 available 4,6-dichloro-2-(methylsulfonyl)pyrimidine.(12) This compound underwent successive
186 additions of aniline to afford 2-(methylsulfonyl)-N^4,N^6-diphenylpyrimidine-4,6-diamine.
187 Displacement of the methanesulfonyl (Ms) group with hydrazine formed 2-hydrazinyl-N^4,N^6-
188 diphenylpyrimidine-4,6-diamine (**A**). Reaction of **A** with the appropriate aldehyde led to 5-
189 nitrofurylhydrazone JSF-2245, furylhydrazone JSF-2246, 5-nitrothienylhydrazone JSF-2275, 4-
190 nitrophenylhydrazone, JSF-2325, and 3-nitrophenylhydrazone JSF-2326. **A** was reacted with 5-
191 nitro-2-furoyl chloride to prepare the hydrazide JSF-2247. Alternatively, 4,6-dichloro-2-
192 (methylsulfonyl)pyrimidine reacted with lithium anilide to afford 4,6-dichloro-*N*-
193 phenylpyrimidin-2-amine. Sequential additions of aniline and hydrazine afforded 6-substituted

hydrazine (**B**). Condensation of **B** with the appropriate aldehyde led to 5-nitrofurylhydrazone JSF-2332, furylhydrazone JSF-2370, 4-nitrophenylhydrazone JSF-2327, and 5-nitrothienylhydrazone JSF-2371. Reaction with 5-nitrofuran-2-carbonyl chloride led to the corresponding hydrazide JSF-2372.

The synthesized pyrimidine analogs were initially assessed for their respective ability to inhibit the growth of *in vitro* cultured *M. tuberculosis* (H37Rv strain) under standard liquid culture conditions (media: Middlebrook 7H9 supplemented with albumin, dextrose, catalase, and glycerol) at 37 °C via an Alamar blue assay (Table 1).(13) An MIC was determined, representing the concentration of compound inhibiting 90% of the growth of the bacteria. To assess cytotoxicity to a model mammalian cell line, we determined the CC_{50} (concentration of compound required to inhibit 50% of the growth of the cells) for each compound versus Vero cells – African Green monkey kidney cells (#ATCC CCL-81).(14) The selectivity index (SI) may be defined as CC_{50}/MIC, and one typically targets an SI $\geq$ 10.

A comparison of the SAR for JSF-2019, JSF-2245 and JSF-2332 demonstrated the 2-hydrazone substituted pyrimidine (JSF-2245) to be essentially equipotent to JSF-2019, while the 6-substituted pyrimidine (JSF-2332) was threefold less active. The Vero cell-based SI values for all three compounds were similar (within a factor of two). Replacement of the 5-nitro substituent with a hydrogen led to a significant loss (140X) of whole-cell activity with 2-hydrazone substituted JSF-2246, while in the 6-hydrazone case an 18-fold loss was realized. Little change in Vero cell cytotoxicity in either series was noted. Similarly, replacements of the 5-nitrofuryl with 5-nitrothienyl (JSF-2275), 4-nitrophenyl (JSF-2325), and 3-nitrophenyl (JSF-2326) led to significant losses in whole-cell activity. Except for JSF-2275 (with a CC_{50} > 120 μM), these analogs also failed to demonstrate a substantial improvement in Vero cell cytotoxicity. The acyl

hydrazide (JSF-2247) was slightly less active (MIC = 0.23 μM), but exhibited significantly more Vero cell cytotoxicity (CC_{50} = 1.8 μM).

The 6-substituted pyrimidine series displayed some similar trends to the 2-substituted series such as the significant loss of whole-cell efficacy when replacing the 5-nitrofuryl group with a 4-nitrophenyl (JSF-2327) or furyl (JSF-2370). Similarly, the hydrazone moiety may not be substituted by a hydrazide (JSF-2372) without an unfavorable change in antitubercular activity. The 5-nitrothienyl analog (JSF-2371), however, did not follow the trend in the 2-substituted series. JSF-2371 exhibited enhanced activity (MIC = 0.11 μM) and reduced cytotoxicity as compared to JSF-2332, strikingly with an SI = 250.

Those compounds with an MIC ≤ 20 μM were also profiled for their cidal activity through determination of the minimum bactericidal concentration (MBC; minimum concentration of compound resulting in a ≥2 $\log_{10}$ decrease in colony-forming units of bacteria grown on solid culture medium) vs. *M. tuberculosis*. While JSF-2019 exhibited an MBC = 0.058 – 0.11 μM, the two most cidal pyrimidines were JSF-2245 (MBC = 0.24 – 0.48 μM) and JSF-2371 (MBC = 0.44 – 0.92 μM). Thus, both analogs may be considered bactericidal given the criteria that the MBC/MIC ≤ 4. The kinetics of cidality for these two compounds were also determined and compared to JSF-2019. JSF-2245 at 30X MIC, somewhat similar to JSF-2019, afforded a >6 $\log_{10}$ kill over 10 d. JSF-2371, at a similar multiple of its MIC, reduced the CFUs by ~ 1 $\log_{10}$ over 10 – 14 d and then a rebound was observed through an outgrowth of persistent and/or resistant bacteria.

The kinetic solubility of the original hit JSF-2019 in phosphate-buffered saline (PBS) at pH 7.4 was determined to be less than 0.06 μM (Table 2). The lack of *in vivo* efficacy of JSF-2019 in a mouse model of *M. tuberculosis* may in part be attributed to its poor solubility. As

expected based on their slightly increased clogP values as compared to JSF-2019, none of the subset of pyrimidine 2- or 4-hydrazones displayed a significantly enhanced aqueous solubility. However, the solubilities in pH 7.4 PBS of hydrazide analogs JSF-2247 and JSF-2372 were determined to be 5.96 and 9.23 μM, respectively.

In parallel, the metabolic stability of the pyrimidines was assessed in the presence of mouse liver microsomal (MLM) preparations for the determination of half-life ($t_{1/2}$) and intrinsic clearance (Cl_{int}) (Table 2). The original hit, JSF-2019, displayed acceptable metabolic stability: $t_{1/2}$ = 63.6 min and Cl_{int} = 10.9 μL/min/mg microsomal protein. Hydrazone JSF-2371 and hydrazide JSF-2372 exhibited greater metabolic stability than JSF-2019. JSF-2245 and JSF-2332, the most similar pyrimidine analogs of JSF-2019, both exhibited significantly diminished $t_{1/2}$ and increased Cl_{int} values as compared to the triazine hit. In an attempt to flag a potential liability downstream of initial animal studies to be conducted in mice, human liver microsomal (HLM) stabilities were also measured for these five pyrimidines and JSF-2019. As expected, JSF-2019 was sufficiently stable ($t_{1/2}$ = 77.9 min) as were pyrimidines JSF-2372 ($t_{1/2}$ = 100 min) and JSF-2371 ($t_{1/2}$ = 68.6 min).

The pharmacokinetic (PK) profile of select pyrimidine analogs in female CD-1 mice via oral (po) administration was determined (Figure 4 and Table 3). Of significance were the exposure of the compound in plasma, related to its area under the curve (AUC) value, and a qualitative determination of how much exposure was above the MIC. In addition, since tuberculosis is primarily a pulmonary disease, the ratio of C_{lung}/C_{plasma} was determined at t = 5 h. For all compounds tested except JSF-2247, this value was >1.0 and deemed acceptable. The AUC of JSF-2019 was determined to be 869.1 h×ng/mL. As shown in Figure 4A, the compound displayed good exposure as both mice had a C_{plasma} that was higher than the MIC (0.0625

μg/mL) over the course of the 5 h study. JSF-2245 and JSF-2371 also exhibited C_{plasma} levels higher than their MIC for more than 3 and 5 h, respectively. Both compounds were determined to have an AUC comparable to that of the original hit (788.5 and 726.4 h×ng/mL, respectively). JSF-2332 demonstrated a similar AUC value, but its C_{plasma} was below the MIC within 1–2 h. The exposure of JSF-2247 (AUC = 534.6 h×ng/mL) was slightly diminished compared to these three pyrimidines and its C_{plasma} dropped below the MIC after 1.5 – 2.5 h. Lastly, the hydrazide analog JSF-2372 had the lowest exposure with C_{plasma} never exceeding its MIC and an AUC of 162.7 h×ng/mL.

JSF-2245 exhibited a favorable PK profile characterized by a slightly greater exposure than JSF-2371, consistent with its higher Caco-2 cell permeability (Table 2).(7) Significantly, however, JSF-2371 exhibited a longer half-life *in vivo*, suggested by its larger MLM $t_{1/2}$. In addition, JSF-2371 exhibited minimal inhibition (IC_{50} values: 4.44 - >50 μM) of human cytochrome P450 enzymes (1A2, 2C9, 2C19, 2D6, and 3A4; Table 4). A concern, however, was its high degree of mouse plasma protein binding (99.98%) and slightly low plasma stability at 5 h (70.0%) (Supplementary Table 2). It is interesting to note that both properties in the presence of human plasma were acceptable (Supplementary Table 2). JSF-2371 was selected for PK profiling via both intravenous (iv) and po administration to obtain the relative oral bioavailability of the compound (Quality control statistics may be found in Supplementary Table 3). A formulation of 5% DMA/4% Cremophor was used for iv administration of JSF-2371. Oral administration involved a formulation of 0.5% CMC/0.5% Tween 80 and resulted in oral bioavailability (F) of 0.5%. Finally, given the significance of *M. tuberculosis* infected macrophages in the lung pathology in mouse models and actual human disease, we determined that JSF-2371 was cidal to the *M. tuberculosis* Δ*leuCD* Δ*panCD* $mc^2$6206 strain infecting J774.1

cells (Supplementary Figure 1). At 1.0 μg/mL, JSF-2371 afforded an ca. two $\log_{10}$ reduction in bacterial colony-forming units (CFUs) as compared to the no-drug control, similar to the rifampicin (5 μg/mL) positive control. A 10 μg/mL concentration of JSF-2371 reduced the bacterial load to below the limit of quantification (~ 0 CFUs).

Efforts to continue the optimization of the pyrimidines are currently in progress, bolstered by these initial results as well as preliminary studies to probe their mechanism of action. Similar to JSF-2019, JSF-2371 largely maintains its *in vitro* activity versus clinical *M. tuberculosis* strains with resistance to one or more of the following approved tuberculosis drugs: isoniazid, rifampicin, ethambutol, kanamycin, streptomycin, and capreomycin (Supplementary Table 4) with 4x resistance in two multi drug-resistant strains. Interestingly, JSF-2371 does not significantly inhibit the growth of the ESKAPE bacteria while JSF-2019 demonstrates a MIC = 2.3 μM versus a clinical methicillin-resistant strain of *S. aureus* (Supplementary Table 5). JSF-2019 and JSF-2245 exhibit cross-resistance (8 – 32 X MIC shift) with laboratory PA-824–resistant strains (Supplementary Table 6) harboring mutations in F_{420} biosynthesis (*fbiB*, *fbiC*)(15, 16) or the F_{420}-dependent glucose-6-phosphate dehydrogenase *fgd1*.(17) Expectedly, JSF-2246, lacking a nitro group, is not cross-resistant with these strains. JSF-2371 intriguingly only exhibits low-level cross-resistance (two-fold MIC shift) with these strains. Additionally, a mutant was generated with a transposon insertion in the PA-824 activating gene *ddn*,(18, 19) and JSF-2019, JSF-2245 and JSF-2371 exhibit different losses in activity (5-, 8-, and 16-fold, respectively) while JSF-2246 lacks cross-resistance.

DISCUSSION

The potential for pyrimidine compounds as novel antitubercular agents has been demonstrated through preliminary SAR studies taking into consideration *in vitro* efficacy, *in vitro* cytotoxicity, physiochemical properties, *in vitro* ADME parameters, and mouse PK profiles. The original hit compound JSF-2019 was discovered through a virtual screening of the GSK set of antimalarials using a dual-event Bayesian machine learning model that simultaneously predicts whole-cell *in vitro* efficacy against *M. tuberculosis* and a relative lack of Vero cell cytotoxicity.(3, 20) Our SAR studies of the compound to improve its activity and PK profiles led to pyrimidine analogs. From our preliminary SAR investigations, it was apparent that the *in vitro* antitubercular efficacy, Vero cell-based SI, and MLM stability of JSF-2019 could be mostly maintained if not improved with analogs JSF-2371 and JSF-2245. However, we were unable concomitantly to improve aqueous solubility; further studies will need to build on the single-digit micromolar solubilities of hydrazides JSF-2247 and JSF-2372. Insight from mouse PK studies assessing compound exposure (two mice judged over a five hour window post a single oral dose of 25 mg/kg) afforded a further critical evaluation of these pyrimidines and established JSF-2371 as the preferred candidate for a more extensive PK profiling. Unfortunately, JSF-2371 demonstrated poor oral bioavailability, which halted its progression to dose tolerability and proportionality studies. Also concerning were its *in vitro* killing kinetic profile demonstrating limited cidality and mouse plasma profile (very high protein binding and borderline stability).

The process of attempting to evolve the triazine JSF-2019 via the pyrimidine series also afforded an opportunity to begin to explore their respective mechanisms of action. A common feature amongst JSF-2019 and pyrimidines such as JSF-2245 and JSF-2371 is their nitroheterocycle (i.e., furan or thiophene). At this juncture, through studies with spontaneous drug-resistant mutants exhibiting PA-824 cross-resistance, we can state that JSF-2019, JSF-2245,

and JSF-2371 may not share the same mechanism of activation as PA-824. From growth inhibition assays with PA-824–resistant strains harboring a mutation in F_{420} biosynthesis (*fbiB* or *fbiC*) or in F_{420} reduction to $F_{420}H_2$ (*fgd1*), we believe that nitrofurans JSF-2019 and JSF-2245 share a similar requirement for the activation of a nitroreductase through $F_{420}H_2$ biosynthesis. Mutations in the biosynthesis of F_{420} (*fbiB* or *fbiC*) lead to significant losses of activity of JSF-2019 (MIC shift of 32-fold) and JSF-2245 (MIC shift of 8–16 fold). However, nitrothiophene JSF-2371 only exhibits a twofold loss of activity. This appears to run counter to its 16-fold loss of activity versus the *tn::ddn* strain. JSF-2019 and JSF-2245 exhibit 5- and 8-fold reductions in activity against the *tn:ddn* strain, suggesting that Ddn may not be the primary nitroreductase pertinent to their activation. Ddn appears to be the primary nitroreductase for PA-824 (MIC shift of >62-fold). Further studies are in progress to probe the mechanism/s of activation of JSF-2019, JSF-2245, and JSF-2371. The opportunity clearly exists to purposefully design antitubercular nitroheterocyclic small molecules with a distinct mode of activation through further optimization of the pyrimidines disclosed herein.

While the optimization to address liabilities of the pyrimidines continues, we assert that lessons are to be learned from our efforts to date. This reported effort has focused on antituberculars, but we suggest that generalization of these lessons to other antibacterials and antimicrobials should be straightforward. From its inception, a program to evolve a chemical tool to validate a mechanism and/or to advance a drug discovery effort should focus on demonstrating *in vivo* activity in the first-line animal model. For tuberculosis research, this model typically involves the mouse, which has been utilized for over seventy years with recognition of its strengths and weaknesses.(21, 22) Workman and Collins have written about the ideal properties for a chemical probe and been guided principally by experiences in the oncology field.(23) We

354 choose to more generally focus on what we term chemical tools, which may or may not exhibit
355 polypharmacology,(24, 25) and may seed a drug discovery effort in addition to increasing our
356 basic understanding of fundamental biology. Rather than relying solely on Lipinski's Rule of
357 Five,(26) which while based on orally bioavailable drugs across many therapeutic areas may best
358 be applied to filtering large libraries for initial screens and/or prioritizing the resulting set of
359 hits,(23) we will suggest guidelines for compound profile parameters for antituberculars that
360 should help usher an optimization towards *in vivo* active compounds. The focus, taking a cue
361 from prior efforts in the pharmaceutical industry,(27) is in profiling activity, cytotoxicity,
362 physiochemical, ADME, and PK properties early to identify and then address chemical tool
363 shortcomings more efficiently.

364 *In vitro* efficacy, which may be measured in a number of assays,(28) is typically a critical
365 requirement for *in vivo* activity and should be present along with an absence of significant *in*
366 *vitro* and *in vivo* toxicity pertinent to the infected host. We assert that most typically an MIC ≤ 1
367 μM is sufficient, although caveats involve the specifics of the growth inhibition assay (bacterial
368 sub-population and what aspects of the host environment are taken into account).(29) The MIC
369 should be at least tenfold smaller than the CC_{50} (SI $\geq$ 10). Since both intracellular and
370 extracellular bacteria characterize an *M. tuberculosis* infection in humans, the results from an
371 infected macrophage assay should be weighed carefully. The active compound must be present
372 *in vivo* at a sufficient concentration for an adequate time window to maintain coverage to inhibit
373 the growth of, or preferably be cidal to, *M. tuberculosis* (MBC/MIC $\leq$ 4; where MBC is the
374 minimum bactericidal concentration equal to the amount of compound resulting in a 2 $\log_{10}$
375 reduction in CFUs, as compared to the no-drug control).(30, 31)

A set of molecular properties has been evolved and shown to correlate with oral bioavailability, given the strong preference for oral administration of tuberculosis drugs.(30) It is critical to work with soluble compounds (pH 7.4 PBS solubility of at least 1 μM if not ≥100 μM) to avoid issues with formulation for *in vivo* studies, as well as with enzyme and cellular assays.(32) MLM stability is crucial ($t_{1/2} \geq 1$ h and $Cl_{int} \leq 10$ μL/min/mg protein) such that the active molecule is not metabolized rapidly in the model host.(33) These microsomal preparations represent the membrane-bound fraction from hepatocytes and predominantly exhibit Phase I metabolic reactivity to provide more soluble and hydrophilic compounds for eventual excretion. Promising compounds in these aforementioned assays should also exhibit favorable Caco-2 cell permeability, prior to study in a mouse infection model. Oral absorption correlates with permeability to these human colon adenocarcinoma cells that form tight junctions and express transporters on the apical (A) and basolateral (B) surfaces.(34) Compounds are considered sufficiently permeable if $P_{A-B} > 10 \times 10^{-6}$ cm/s and P_{B-A}/P_{A-B} should be ≤ 3, indicating a lack of active efflux.(30) While these *in vitro* ADME assays are critical, the significance of the mouse PK studies cannot be understated. The two mice/five h studies with a single oral dose of compound allow a rough determination of compound exposure and help prioritize compounds by their AUC_{0-t}, C_{max}, and $t_{1/2}$. The goal is to generally maximize these parameters unless they are associated with toxicity. While the reduction of *M. tuberculosis* burden in mice does not correlate with one specific PK or PK/PD index, it certainly would seem to require a basal level of oral exposure.(29)

Thus, the evolution of the pyrimidines and other concurrent programs in our laboratories have helped clarify key *in vitro* activity and cytotoxicity, physiochemical, *in vitro* ADME, and *in vivo* PK parameters and their target values to increase the likelihood of arriving at small

molecule antituberculars with sufficient exposure when dosed orally in the mouse model. This represents a multiple-objective optimization.(35) While JSF-2371 fell short of this target oral exposure, it has reinforced the need to probe structural variations of the compound to meet this goal. Upon achieving significant oral exposure, the compound will then offer the opportunity to demonstrate that its mechanism of action does modulate one or more novel mycobacterial targets of therapeutic relevance, as seen by a significant *in vitro* reduction in bacterial load post-dosing regimen.

ACKNOWLEDGEMENTS

Professor William R. Jacobs, Jr. (Albert Einstein College of Medicine) is thanked for the kind donation of the mc^{2}6206 strain and Professor Jeffrey S. Cox (UC Berkeley) is acknowledged for the gracious donation of the mLux plasmid. Mr. Xin Wang (Rutgers University) and Dr. Sean Ekins (Collaborations Pharmaceuticals) is thanked for his critical comments during the course of this project.

ETHICS STATEMENT

All animal studies were ethically reviewed and carried out in accordance with the Guide for the Care and Use of Laboratory Animals of the National Institutes of Health, with approval from the Institutional Animal Care and Use Committee (IACUC) of the New Jersey Medical School, Rutgers University, Newark.

FUNDING INFORMATION

This work was supported by the NIH grant U19AI109713.

423 **REFERENCES**

424 1. Global Tuberculosis Report 2016, *on* World Health Organization.
425 http://www.who.int/tb/publications/global_report/en/.

426 2. Cooper CB. 2013. Development of Mycobacterium tuberculosis Whole Cell Screening
427 Hits as Potential Antituberculosis Agents. J Med Chem 56:7755-7760.

428 3. Ekins S, Reynolds Robert C, Kim H, Koo M-S, Ekonomidis M, Talaue M, Paget Steve D,
429 Woolhiser Lisa K, Lenaerts Anne J, Bunin Barry A, Connell N, Freundlich Joel S. 2013.
430 Bayesian Models Leveraging Bioactivity and Cytotoxicity Information for Drug
431 Discovery. Chem Biol 20:370-378.

432 4. Lenaerts AJM, Gruppo V, Brooks JV, Orme IM. 2003. Rapid In Vivo Screening of
433 Experimental Drugs for Tuberculosis Using Gamma Interferon Gene-Disrupted Mice.
434 Antimicrob Agents Chemother 47:783-785.

435 5. Li S-G, Vilchèze C, Chakraborty S, Wang X, Kim H, Anisetti M, Ekins S, Rhee KY,
436 Jacobs WR, Freundlich JS. 2015. Evolution of a thienopyrimidine antitubercular relying
437 on medicinal chemistry and metabolomics insights(). Tetrahedron Lett 56:3246-3250.

438 6. Kerns EH, Di L. 2008. Drug-like Properties: Concepts, Structure Design and Methods:
439 from ADME to Toxicity Optimization. Elsevier, Amsterdam.

440 7. Hubatsch I, Ragnarsson EGE, Artursson P. 2007. Determination of drug permeability and
441 prediction of drug absorption in Caco-2 monolayers. Nat Protocols 2:2111-2119.

442 8. Krieger Inna V, Freundlich Joel S, Gawandi Vijay B, Roberts Justin P, Gawandi
443 Vidyadhar B, Sun Q, Owen Joshua L, Fraile Maria T, Huss Sofia I, Lavandera J-L,
444 Ioerger Thomas R, Sacchettini James C. 2012. Structure-Guided Discovery of Phenyl-
445 diketo Acids as Potent Inhibitors of M. tuberculosis Malate Synthase. Chem Biol
446 19:1556-1567.

447 9. Mahmud K, Raffaele L, Dino M, Federica V, Monica R, Stefano F, Kevin DR. 2011. A
448 Comparative Study of the CYP450 Inhibition Potential of Marketed Drugs Using Two
449 Fluorescence Based Assay Platforms Routinely Used in the Pharmaceutical Industry.
450 Drug Metabolism Letters 5:30-39.

451 10. Mehta PK, King CH, White EH, Murtagh JJ, Quinn FD. 1996. Comparison of in vitro
452 models for the study of Mycobacterium tuberculosis invasion and intracellular replication.
453 Infect Immun 64:2673-9.

454 11. Rengarajan J, Bloom BR, Rubin EJ. 2005. Genome-wide requirements for
455 Mycobacterium tuberculosis adaptation and survival in macrophages. Proc Natl Acad Sci
456 U S A 102:8327-8332.

12. Baiazitov R, Du W, Lee C-S, Hwang S, Almstead NG, Moon Y-C. 2013. Chemoselective Reactions of 4,6-Dichloro-2-(methylsulfonyl)pyrimidine and Related Electrophiles with Amines. Synthesis 45:1764-1784.

13. Cho S, Lee HS, Franzblau S. 2015. Microplate Alamar Blue Assay (MABA) and Low Oxygen Recovery Assay (LORA) for Mycobacterium tuberculosis, p 281-292. *In* Parish T, Roberts MD (ed), Mycobacteria Protocols doi:10.1007/978-1-4939-2450-9_17. Springer New York, New York, NY.

14. Vilchèze C, Baughn AD, Tufariello J, Leung LW, Kuo M, Basler CF, Alland D, Sacchettini JC, Freundlich JS, Jacobs WR. 2011. Novel Inhibitors of InhA Efficiently Kill Mycobacterium tuberculosis under Aerobic and Anaerobic Conditions. Antimicrob Agents Chemother 55:3889-3898.

15. Choi KP, Bair TB, Bae YM, Daniels L. 2001. Use of transposon Tn5367 mutagenesis and a nitroimidazopyran-based selection system to demonstrate a requirement for fbiA and fbiB in coenzyme F(420) biosynthesis by Mycobacterium bovis BCG. J Bacteriol 183:7058-66.

16. Choi KP, Kendrick N, Daniels L. 2002. Demonstration that fbiC is required by Mycobacterium bovis BCG for coenzyme F(420) and FO biosynthesis. J Bacteriol 184:2420-8.

17. Stover CK, Warrener P, VanDevanter DR, Sherman DR, Arain TM, Langhorne MH, Anderson SW, Towell JA, Yuan Y, McMurray DN, Kreiswirth BN, Barry CE, Baker WR. 2000. A small-molecule nitroimidazopyran drug candidate for the treatment of tuberculosis. Nature 405:962-966.

18. Manjunatha UH, Boshoff H, Dowd CS, Zhang L, Albert TJ, Norton JE, Daniels L, Dick T, Pang SS, Barry III CE. 2006. Identification of a nitroimidazo-oxazine-specific protein involved in PA-824 resistance in *Mycobacterium tuberculosis*. Proc Natl Acad Sci 103:431-436.

19. Singh R, Manjunatha U, Boshoff HI, Ha YH, Niyomrattanakit P, Ledwidge R, Dowd CS, Lee IY, Kim P, Zhang L, Kang S, Keller TH, Jiricek J, Barry CE, 3rd. 2008. PA-824 kills nonreplicating Mycobacterium tuberculosis by intracellular NO release. Science 322:1392-5.

20. Gamo F-J, Sanz LM, Vidal J, de Cozar C, Alvarez E, Lavandera J-L, Vanderwall DE, Green DVS, Kumar V, Hasan S, Brown JR, Peishoff CE, Cardon LR, Garcia-Bustos JF. 2010. Thousands of chemical starting points for antimalarial lead identification. Nature 465:305-310.

21. Ekins S, Nuermberger EL, Freundlich JS. 2014. Minding the gaps in tuberculosis research. Drug Discovery Today 19:1279-1282.

22. Ekins S, Pottorf R, Reynolds RC, Williams AJ, Clark AM, Freundlich JS. 2014. Looking Back to the Future: Predicting in Vivo Efficacy of Small Molecules versus Mycobacterium tuberculosis. J Chem Inf Model 54:1070-1082.

23. Workman P, Collins I. 2010. Probing the Probes: Fitness Factors For Small Molecule Tools. Chem Biol 17:561-577.

24. Tan Z, Chaudhai R, Zhang S. 2016. Polypharmacology in Drug Development: A Minireview of Current Technologies. ChemMedChem doi:10.1002/cmdc.201600067:n/a-n/a.

25. Anighoro A, Bajorath J, Rastelli G. 2014. Polypharmacology: Challenges and Opportunities in Drug Discovery. J Med Chem 57:7874-7887.

26. Lipinski CA, Lombardo F, Dominy BW, Feeney PJ. 2001. Experimental and computational approaches to estimate solubility and permeability in drug discovery and development settings1. Advanced Drug Delivery Reviews 46:3-26.

27. Kola I, Landis J. 2004. Can the pharmaceutical industry reduce attrition rates? Nat Rev Drug Discov 3:711-716.

28. Franzblau SG, DeGroote MA, Cho SH, Andries K, Nuermberger E, Orme IM, Mdluli K, Angulo-Barturen I, Dick T, Dartois V, Lenaerts AJ. 2012. Comprehensive analysis of methods used for the evaluation of compounds against Mycobacterium tuberculosis. Tuberculosis 92:453-488.

29. Dartois V, Barry 3rd CE. 2013. A medicinal chemists' guide to the unique difficulties of lead optimization for tuberculosis. Bioorg Med Chem Lett 23:4741-4750.

30. Lakshminarayana SB, Huat TB, Ho PC, Manjunatha UH, Dartois V, Dick T, Rao SPS. 2015. Comprehensive physicochemical, pharmacokinetic and activity profiling of anti-TB agents. J Antimicrob Chemother 70:857-867.

31. Xie Z, Siddiqi N, Rubin EJ. 2005. Differential Antibiotic Susceptibilities of Starved Mycobacterium tuberculosis Isolates. Antimicrob Agents Chemother 49:4778-4780.

32. McGovern SL, Helfand BT, Feng B, Shoichet BK. 2003. A Specific Mechanism of Nonspecific Inhibition. J Med Chem 46:4265-4272.

33. Perryman AL, Stratton TP, Ekins S, Freundlich JS. 2016. Predicting Mouse Liver Microsomal Stability with "Pruned" Machine Learning Models and Public Data. Pharm Res 33:433-449.

34. Artursson P, Palm K, Luthman K. 2001. Caco-2 monolayers in experimental and theoretical predictions of drug transport. Adv Drug Deliv Rev 46:27-43.

35. Ekins S, Honeycutt JD, Metz JT. 2010. Evolving molecules using multi-objective optimization: applying to ADME/Tox. Drug Discovery Today 15:451-460.

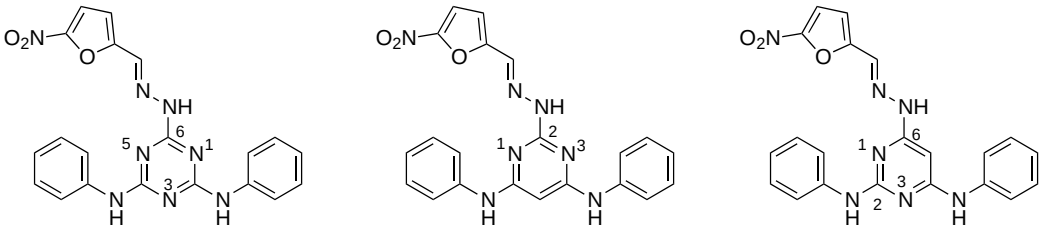

FIG 1 Structure of JSF-2019 and its two pyrimidine analogs.

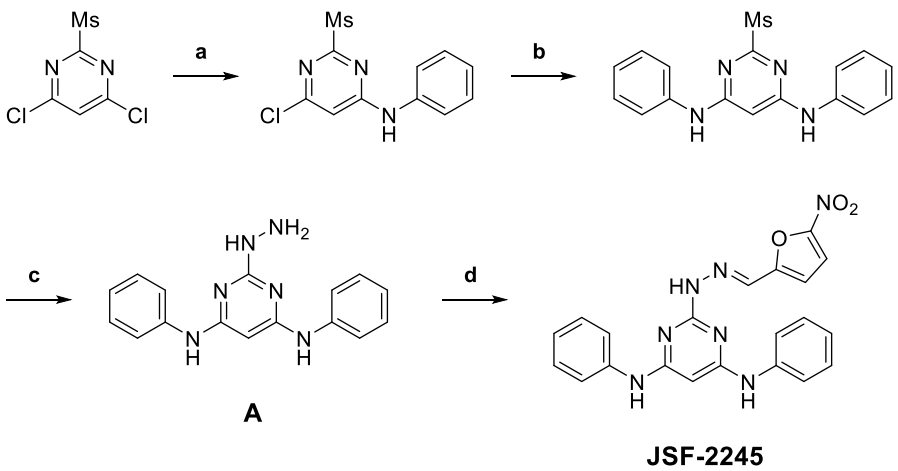

FIG 2 Synthetic route to JSF-2245: (a) $PhNH_2$, 2,6-lutidine, DMSO, rt; (b) $PhNH_2$, 2,6-lutidine, DMSO, rt; (c) NH_2NH_2, DMSO, 70 °C; (d) 5-nitro-2-furaldehyde, MeOH, rt.

537
538

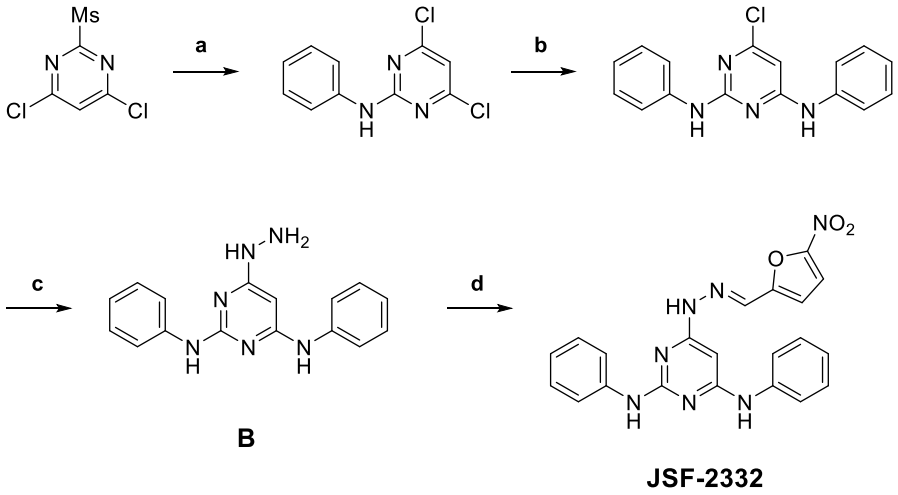

539
540
541 **FIG 3** Synthetic route to JSF-2332: (a) $PhNH_2$, LiHMDS, THF, -78 ˚C; (b) $PhNH_2$, 2,6-lutidine,
542 DMSO, 60 °C; (c) NH_2NH_2, DMSO, 70 °C; (d) 5-nitro-2-furaldehyde, MeOH, rt.
543
544

545

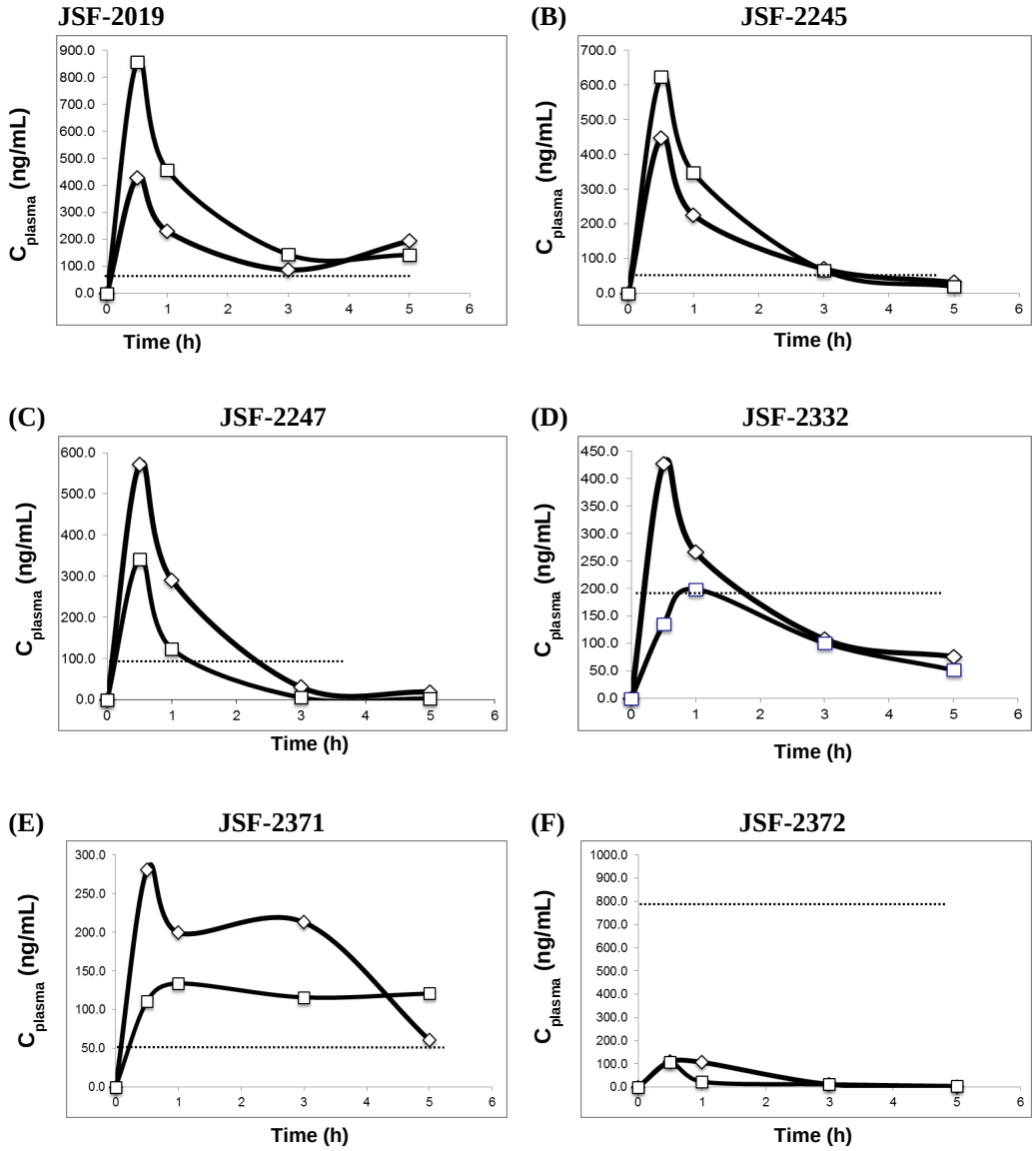

546 **FIG 4** The concentration of compound (C_{plasma}) plotted as a function of time in mouse #1 (◊) and
547 mouse #2 (□) for (A) JSF-2019, (B) JSF-2245, (C) JSF-2247, (D) JSF-2332, (E) JSF-2371, and
548 (F) JSF-2372. The dashed lines indicate the approximate MIC of each compound.
549
550

Table 1 Chemical structure, minimum inhibitory concentration (MIC) against the H37Rv *M. tuberculosis* strain, minimum bactericidal concentration (MBC) against the H37Rv *M. tuberculosis* strain, and Vero cell cytotoxicity (CC_{50}) of pyrimidine compounds

Compound	Structure	*M. tuberculosis* MIC in μg/mL (μM)	*M. tuberculosis* MBC[a] in μg/mL (μM)	Vero cell CC_{50} in μg/mL (μM)
TCMDC-125802 (JSF-2019)	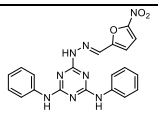	0.062 (0.15)	0.024 – 0.049 (0.058 – 0.11)	4.0 (9.6)
JSF-2245	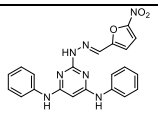	0.049 (0.12)	0.098 – 0.20 (0.24 – 0.48)	3.1 (7.5)
JSF-2246	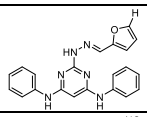	6.2 (17)	25 – 50 (67 – 130)	6.2 (17)
JSF-2247	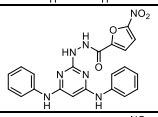	0.098 (0.23)	0.39 – 0.78 (0.90 – 1.8)	0.78 (1.8)
JSF-2275	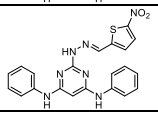	> 50 (>120)	N.D.	> 50 (>120)
JSF-2325	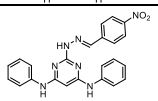	> 50 (>120)	N.D.	6.2 (15)
JSF-2326	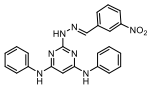	12 (28)	N.D.	1.6 (3.8)
JSF-2327	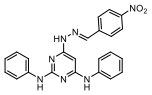	> 50 (>120)	N.D.	25 (59)
JSF-2332	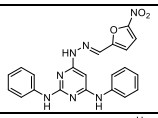	0.19 (0.46)	0.39 – 0.78 (0.94 – 1.9)	6.2 (15)
JSF-2370	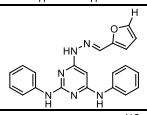	3.1 (8.4)	>50 (>130)	12 (32)
JSF-2371	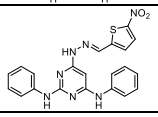	0.048 (0.11)	0.19 – 0.39 (0.44 – 0.92)	12 (28)

JSF-2372	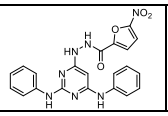	0.78 (1.8)	1.6 – 3.1 (3.7 – 7.2)	12 (28)

[a] N.D. = Not determined

557 **Table 2 Physiochemical properties and *in vitro* Absorption-Distribution-Metabolism-**
558 **Excretion (ADME) profile of select compounds**

	JSF-2019	**JSF-2245**	**JSF-2247**	**JSF-2332**	**JSF-2371**	**JSF-2372**
Kinetic solubility in pH 7.4 PBS (μM)	<0.06	0.0605	5.96	< 0.06	< 0.06	9.23
MLM Stability $t_{1/2}$ (min)	63.6	25.1	26.6	42.5	65.4	70.0
MLM Stability Cl_{int} (μL/min/mg protein)	10.9	27.6	26.1	16.3	10.6	9.9
HLM Stability $t_{1/2}$ (min)	77.9	35.4	59.2	55.5	68.6	100
HLM Stability Cl_{int} (μL/min/mg protein)	8.90	19.6	11.7	12.5	10.1	6.90
Caco-2 cell P_{A-B} / P_{B-A} (x 10^{-6} cm/s)	1.53 / 4.10	15.1 / 9.31	N.D. [a]	2.27 / 0.297	0.0279 / 0.0152	N.D. [a]

559 [a]Not determined
560

Table 3 Mouse PK data for select compounds

	JSF-2019	JSF-2245	JSF-2247	JSF-2332	JSF-2371	JSF-2372
AUC [a] (h*ng/mL)	869.1	788.5	534.6	704.1	726.4	162.7
C_{max} [a] (ng/mL)	317	535	456	281	196	109
MIC (ng/mL)	62	49	98	190	48	780
AUC/MIC [a]	14	16	5.5	3.7	15	0.21
C_{max}/MIC [a]	5.1	11	4.7	1.5	4.1	0.14
T > MIC [a] (h)	5.0	4.0	1.5	2.0	5.0	0
C_{lung}/C_{plasma} at 5 h	2.6	2.6	0.3	6.0	1.0	1.0
$t_{1/2}$ (h) [b]	n.d.	n.d.	n.d.	n.d.	0.86	n.d.
Clearance [b]	n.d.	n.d.	n.d.	n.d.	1436	n.d.
V_d (L/kg) [b]	n.d.	n.d.	n.d.	n.d.	1.34	n.d.

[a]Following administration of a single 25 mg/kg po dose

[b]Following administration of a single 5 mg/kg iv dose

n.d. = not determined

568 **Table 4 *In vitro* inhibition data of human cytochrome P450 isoforms by JSF-2371**

CYP	1A2	2C9	2C19	2D6	3A4
Substrate (Concentration in μM)	phenacetin (10)	diclofenac (10)	omeprazole (0.5)	dextromethorphan (5)	testosterone (100)
Inhibitor Control	naphthoflavone	sulfaphenazole	tranylcypromine	quinidine	ketoconazole
Compounds	**IC_{50} (μM)**	**IC_{50} (μM)**	**IC_{50} (μM)**	**IC_{50} (μM)**	**IC_{50} (μM)**
Inhibitor Control	0.141	0.645	2.31	0.0406	0.0310
JSF-2371	4.44	12.9	19.7	>50	23.3

569

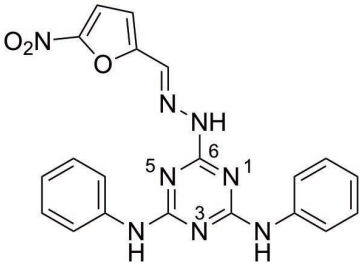

JSF-2019

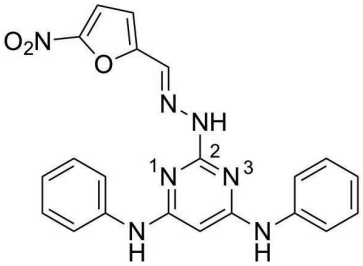

JSF-2245

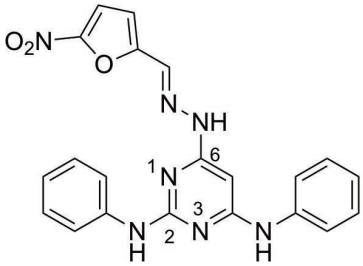

JSF-2332